Chemosphere 298 (2022) 134272

Contents lists available at ScienceDirect

Chemosphere

journal homepage: www.elsevier.com/locate/chemosphere

# Assessment of the link between atmospheric dispersion and chemical composition of $PM_{10}$ at 2-h time resolution

C. Perrino [a,*], M. Giusto [a], T. Sargolini [a], G. Calzolai [b], S. Canepari [a,c]

[a] C.N.R. Institute of Atmospheric Pollution Research, Monterotondo St., Rome, 00015, Italy
[b] INFN National Institute of Nuclear Physics, Florence Section, Sesto Fiorentino, 50019, Italy
[c] Sapienza University of Rome, Environmental Biology Department, Rome, 00185, Italy

## HIGHLIGHTS

- We measured the time pattern of the main $PM_{10}$ components at 2-h time resolution.
- We obtained the mass closure and studied the time pattern of $PM_{10}$ macro-sources.
- Natural radioactivity monitoring efficiently described the mixing depth of the PBL.
- We studied the link between 2-h patterns of PM components and natural radioactivity.
- The time pattern of most PM components shows a clear dependance on PBL mixing depth.

## GRAPHICAL ABSTRACT

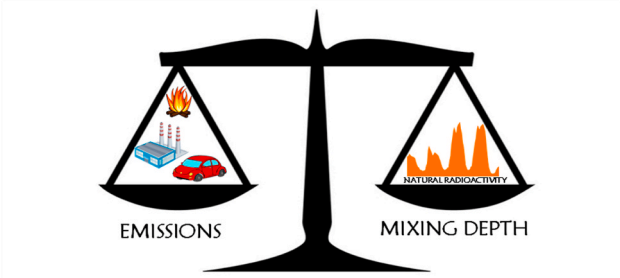


## ARTICLE INFO

Handling Editor: Volker Matthias

*Keywords:*
Natural radioactivity
PM sources
Mass closure
Mixing layer height
Daily cycle

## ABSTRACT

The concentration of air pollutants is governed by both emission rate and atmospheric dispersion conditions. The role played by the atmospheric mixing height in determining the daily time pattern of PM components at the time resolution of 2 h was studied during 21 days of observation selected from a 2-month field campaign carried out in the urban area of Rome, Italy.

Natural radioactivity was used to obtain information about the mixing properties of the lower atmosphere throughout the day and allowed the identification of advection and stability periods. $PM_{10}$ composition was determined by X-ray fluorescence, ion chromatography, inductively coupled plasma-mass spectrometry and thermo-optical analysis. A satisfactory mass closure was obtained on a 2-h basis, and the time pattern of the $PM_{10}$ macro-sources (soil, sea, secondary inorganics, organics, traffic exhaust) was acquired at the same time scale.

After a complete quality control procedure, 27 main components and source tracers were selected for further elaboration. On this database, we identified some groups of co-varying species related to the main sources of PM. Each group showed a peculiar behaviour in relation to the mixing depth. PM components released by soil, biomass burning and traffic exhaust, and, particularly, ammonium nitrate, showed a clear dependence on the mixing properties of the lower atmosphere. Biomass burning components and organics peaked during the night hours (around midnight), following the atmospheric stabilization and increased emission rate. Traffic exhausts and non-exhausts species also peaked in the evening, but they showed a second, minor increase between 6:00 and 10:00 when the strengthening of the emission rate (morning rush hour) was counterbalanced by the dilution of

* Corresponding author.
*E-mail address:* perrino@iia.cnr.it (C. Perrino).

https://doi.org/10.1016/j.chemosphere.2022.134272
Received 8 November 2021; Received in revised form 21 February 2022; Accepted 7 March 2022
Available online 12 March 2022

the atmosphere (increasing mixing depth). In the case of ammonium nitrate, high concentrations were kept during the whole night and morning.

## 1. Introduction

As well known, the atmospheric concentration of any pollutant is the result of the interaction between the mass amount released by its sources, its reaction/deposition rate, and the air volume available for its dispersion. To explain the time pattern of pollutants concentration and to evaluate the time variations in the strength of their sources, it is thus necessary to estimate also the variations in the height of the Planetary Boundary Layer (PBL), that is, the lowest part of the atmosphere that is directly influenced by its contact with the Earth surface, where pollutants are dispersed.

In high-pressure conditions, the height of the PBL changes according to a typical daily cycle. During day hours, vertical mixing is strong because of turbulence, and the PBL may reach a height of a few kilometres. In these conditions, chemical species released into the PBL gradually disperse in all directions and, in the absence of significant sinks and after sufficient time, become thoroughly mixed in the so-called convective mixing layer. In the ideal case of constant emission sources, during the central hours of the day the concentration of pollutants is generally at a minimum. Convective turbulence progressively softens at sunset, and a stable layer develops close to the ground, with a residual layer above. In these conditions, pollutants emitted from the surface are trapped in the stable layer, which can be as low as some tens of meters, reaching their maximum concentration (Seibert et al., 2000; Vecchi et al., 2019). Low pollutant concentration is observed not only in high-pressure conditions, during the vertical dilution phase caused by increased PBL depth, but also in horizontal advection conditions, when the air masses, generally cleaner, are transported from outside the city.

As the PBL usually responds to changes in surface radiative forcing in the time of about an hour (Stull, 1988) and the intensity of emission sources may vary rapidly as well, to interpret the variations in the concentration of air pollutants it is necessary to determine both mixing height and pollutants concentration at high time-resolution.

The height of the mixing layer is traditionally evaluated by remote sensing techniques (lidar, sodar, radar), vertical profile measurements (tethered balloons, radiosondes) or numerical models (Vogelezang and Holtslag, 1996; Seibert et al., 2000; Nath and Patil, 2006; Emeis et al., 2008). Besides, many authors have indicated the determination of natural radioactivity due to Radon ($^{222}$Rn) or Radon daughters as a simple and effective tool for describing mixing height variations (Guedalia et al., 1980; Allegrini et al., 1994; Duenas et al., 1996; Perrino et al. 2001, 2008, 2010, 2015; Pasini et al., 2003; Sesana et al., 2003; Desideri et al., 2006; Griffith et al., 2013; Chambers et al., 2015; Salzano et al., 2016; Wang et al., 2016; Williams et al., 2016; Gregoric et al., 2020).

Radon, a radioactive natural gas belonging to the series of $^{238}$U, is emitted from soil and rocks and is distributed in the atmosphere by turbulent mixing (Porstendorfer, 1994). Its only transformation is the radioactive decay into daughter radionuclides (half-life: 3.82 days). Radon exhalation rate depends on the geological characteristics of the area and may change only in the case of snow or ice cover (Gregoric et al., 2020), which are extremely rare in Rome and did not occur during the Special Observation Periods of this study. Therefore, in the temporal and spatial scale of our observations (a few weeks, several kilometres), the variations in Radon exhalation rate can be neglected. Because of their electric charge, daughter radionuclides rapidly fix to atmospheric particles, where their radioactivity can be measured, also at high time-resolution (Porstendorfer, 1994). Natural radioactivity due to Radon progeny increases when atmospheric stability increases and decreases during advection or when the atmospheric convective mixing is efficient. It can be successfully used for uncoupling concentration variations due to changes in pollutant emission/transformation rate from those due to changes in the mixing properties of the boundary layer.

The interpretation of variability in pollutants concentration is particularly challenging in the case of particulate matter (PM). Each chemical component of PM has its sources, size distribution, typical shape, reaction pathways and deposition rate, and, consequently, its concentration shows an individual daily cycle. To clarify the link between mixing properties of the boundary layer and PM concentration, it is thus necessary to measure the main PM chemical components individually. Some attempts to study the relationship between chemical composition of PM and atmospheric mixing have been previously carried out but, to our knowledge, most of these studies considered 24-h average concentration (Perrino et al., 2008) or focused on specific PM components, e.g. elements (Kidwell and Ondov, 2004; Nicolas et al., 2020) or elements and ions (Perrino et al., 2010). In contrast, the many studies about PM composition at high time-resolution were focused on the identification of PM sources, but, in most cases, they did not specifically address the role of PBL height variations (D'Alessandro et al., 2003; Pancras et al., 2016; Gao et al., 2016; Bigi et al., 2017; Belis et al., 2019; Li et al., 2020). A first attempt to use information about the atmospheric mixing to interpret PM composition data was made by Vecchi et al. (2009) in the urban area of Milan (Po valley, Italy), considered one of the main pollution hot spots in Europe.

We report in this paper the result of a study carried out at an urban site in Rome, Italy, during February–March 2018. We detected natural radioactivity due to Radon progeny with a time resolution of 1-h and simultaneously measured $PM_{10}$ concentration and its chemical composition (elements, ions, elemental carbon, organic carbon) for 51 days with a time resolution of 24 h and for 21 selected days of the same period with a time resolution of 2 h. The measurement of all the main $PM_{10}$ components allowed us to obtain a satisfactory mass closure on a 2-h basis. The main goal of the study was to highlight the role of dispersion in determining the daily time pattern of $PM_{10}$ chemical components in different atmospheric mixing conditions. Chemical components were studied both individually and grouped into main PM macro-sources.

## 2. Experimental

### 2.1. Study site and period

The samplings were carried out inside the area of the Sapienza University of Rome, at about 80 m from the nearest urban road and close to the Botanical Garden (Google Coordinates: 41°54′8.87″N 12°31′3.83″E; Supplementary Material Figure S1). The city of Rome has a surface area of 1285 km$^2$ and about 2.850 million inhabitants. It is located on the west coast of Italy, about 25 km from the Tyrrhenian Sea. It is characterized by heavy traffic, with more than 600 vehicles and 130 motorcycle every 1000 inhabitants (Comune di Roma, 2017). Its economy is primarily dominated by services and some small-medium enterprises, and there are no heavy industries.

The overall study period was from February 6th to March 29th, 2018. During this interval, we continuously measured natural radioactivity on a 1-h basis and $PM_{10}$ concentration on a 24-h basis. According to the weather forecast, we identified possible periods of interest in this time span and activated 2-h samplings on February 7–10 and 16–18 and March 8–14 and 22–28, for a total of 21 days (Special Observation Periods, SOPs). We included in these SOPS some days characterised by anticyclonic conditions and persistent temperature inversion, a condition that is not frequent in Rome, but can be useful to obtain a better comprehension of the variation in the daily time pattern of $PM_{10}$ chemical components.

### 2.2. Equipment

Natural radioactivity was measured on a 1-h time basis using an automated monitor (PBL Mixing Monitor, FAI Instruments, Fonte Nuova, Rome - IT). The monitor consists of a PM sampler equipped with a Geiger–Muller counter for determining the total beta activity of the short-lived Radon progeny. The instrument operates on two filters at the same time: while sampling is performed on one filter (1 h), a second filter undergoes the measurement of the short-lived beta activity of the particles (1 h, a period long enough to guarantee good accuracy of the results; residual radioactivity is taken into account by a software procedure). It is worth noting that the disequilibrium between radon and its progeny may slightly change as a function of the atmospheric stability, and this may constitute a small source of uncertainty in the data interpretation, particularly under anti-cyclonic conditions.

24-h $PM_{10}$ concentration was measured, from midnight to midnight, using a beta attenuation dual-channel automatic monitor operating at 2.3 $m^3\ h^{-1}$ (SWAM5a Dual Channel Monitor, FAI Instruments, Fonte Nuova, Rome, IT). The two channels were equipped with Teflon membrane filters (TEFLO, 47 mm, 2.0 μm pore size, PALL Life Sciences) and quartz fibre filters (TISSUQUARTZ 2500QAT, 47 mm, PALL Life Sciences). The instrument is certified as a beta monitor by both TÜV and CERT and is compliant with EU equivalence criteria for PM measurements (EN 12341 and EN 14907 reference methods) (TÜV, 2018).

1-h PM concentration was measured using a SWAM5a Dual Channel Monitor operating in hourly mode. In this version of the instrument, the distances between the beta source, the collection filter and the detector have been kept to a minimum, and the beta spot area has been considerably reduced, obtaining a limit of detection of 2 $\mu g\ m^{-3}$ (1-h). The two channels of the monitor were equipped with $PM_{10}$ and $PM_{2.5}$ sampling heads.

2-h $PM_{10}$ samples were collected by a dual-channel sampler (Hydra Dual Sampler, FAI Instruments, Fonte Nuova, Rome – IT) operating at 2.3 $m^3\ h^{-1}$ on one channel only, equipped with Teflon filters (same as for 24-h samplings).

Elemental and Organic carbon (EC, OC) were determined on a 2-h time basis (sampling: 105 min, analysis 15 min) by using a Field Thermo-Optical Analyser (Sunset Laboratory, OR, U.S.A.) and the NIOSH-QUARTZ temperature protocol.

All the instruments were accommodated into a temperature-controlled van (PBL Mixing Monitor, 1-h and 24-h SWAM Dual Channel Monitor, EC/OC Analyzer) or immediately outside, into a dedicated temperature-controlled housing (Hydra Dual Sampler). The inlets of all the instruments were at about 2.5 m above ground level.

### 2.3. Analytical procedure

The 2-h and 24-h samples collected on Teflon filters were analyzed for their elemental content (Na, Mγ, Al, Si, S, Cl, K, Ca, Ti, Fe) by energy-dispersion X-ray fluorescence (XRF) (XEPOS, Spectro Analytical Instruments, Kleve, D). After, they were extracted for 20 min under sonication in 8 ml deionized water. A 3 ml aliquot was analyzed for its ionic content (chloride, nitrate, sulphate, sodium, potassium, ammonium, magnesium, calcium) by ion chromatography (IC) (ICS1000, Dionex Co., CA, USA). The extract was then filtered using cellulose nitrate filters (0.45 pore size) and analyzed for the soluble fraction of elements (Al, As, B, Ba, Bi, Ca, Cd, Ce, Co, Cr, Cs, Cu, Fe, La, Li, Mg, Mn, Mo, Na, Ni, Pb, Rb, Sb, Sn, Sr, Tl, V, Zn) by Inductively Coupled Plasma Optical Emission Spectrometry with mass detection (ICP-MS) (Brucker 820-MS). We chose to analyze only the soluble fraction of elements ($ICP_{sol}$) because the acid digestion procedure for the analysis of the total elemental content was not suitable for the very low PM amount typically collected in 2 h (sampling volume: 4.6 $m^3$) (Canepari et al., 2009; Perrino et al., 2010).

The 24-h quartz filters were analyzed for EC and OC by thermo-optical analysis (TOA) (OCEC Carbon Aerosol Analy. zer, Sunset Laboratory, OR USA), selecting the same temperature protocol used for the 2-h field instrument.

The limit of detections (LODs) of all analytes for 2-h and 24-h samplings are reported in Supplementary Material Table S1.

### 2.4. Macro-sources

PM macro-components, defined as the chemical species that typically constitute more than 1% of the PM mass, can be grouped in five main clusters (macro-sources), including the main, ubiquitous PM sources: *soil, sea, secondary inorganics, traffic exhaust, organics*. The contribution of the macro-sources was calculated as reported in Farao et al. (2014) and Perrino et al. (2014).

Briefly, the contribution of *soil* was calculated by adding the concentration of the elements that are generally contained in mineral dust: Al, Si, Fe, the insoluble fractions of K, Mg, and Ca, calcium and magnesium carbonate. The insoluble fractions of K, Mg, and Ca were calculated as the difference between the values determined by XRF (total) and IC (soluble fraction); all the elements were considered as oxides (Chow et al., 2015); carbonate ion was calculated as the sum of $Ca^{++}$ multiplied by 1.5 and $Mg^{++}$ multiplied by 2.5. The contribution of *sea* was calculated from the sum of $Na^+$ and $Cl^-$, multiplied by 1.176 to take minor sea-water components into account. *Secondary inorganics* (formed from gas-to-particle conversion processes in the atmosphere) were calculated as the sum of non-sea-salt sulphate, nitrate, and ammonium. The contribution of road *traffic exhaust* was estimated by adding EC to the same amount multiplied by 1.1, to account for organic species that coat the surface of elemental carbon particles (Castro et al., 1999). The remaining OC was considered as *organics*. To take non-C atoms into account, OC concentration was multiplied by 1.6, a factor used in previous studies for urban sites (Chow et al., 2015; Perrino et al., 2016).

### 2.5. Quality control

The overall sampling, analytical and data elaboration procedure on 24-h samples was fully validated in previous papers (Canepari et al., 2006, 2009; Perrino et al., 2010; Farao et al., 2014).

Instead, the chemical analysis of PM components on 2-h samples still constitutes a challenge for the very low amounts collected on the filters, particularly during the central hours of the day. As a first step, we removed from the dataset all the analytes showing more than 50% of data below the LOD ($ICP_{sol}$ analysis of Al, As, B, Bi, Ca, Cd, Ce, Co, Cr, Fe, La, Li, Ni, Pb, Tl, Zn). Afterwards, to check the robustness of our results, for each day we compared the 24-h concentration with the mean concentration of the twelve corresponding 2-h samples (self-consistency test). The results of the linear regression analysis obtained for the β attenuation, XRF, IC, TOA and $ICP_{sol}$ determinations are reported in Table 1. The days when more than four 2-h data were below the detection limit were not included in the dataset. The number N of data pairs used for each regression analysis is reported in the last column.

We obtained satisfactory results in all cases, with slopes in the range 0.82–1.09 and $R^2$ values in the range 0.94–0.99. The worse results were obtained for OC, with a slope of 0.86, and some elements (Ba, Mn, Sr). In these cases, the 2-h data were systematically higher than 24-h data, probably due to the higher relative weight of operative blank values.

In the case of Sb, the ICP analysis of the soluble fraction showed some very high and narrow concentration peaks of unknown sources, recorded during some night periods (up to 38 ng $m^{-3}$ on a 2-h basis). These high concentrations affected both 24-h and 2-h samples and were considered when evaluating the self-consistency. However, in the following data elaboration aimed to discuss the daily concentration pattern, these values were considered as outliers.

A further quality control procedure consisted of an inter-technique comparison. Supplementary Material Table S2 reports the results of the regression analysis for the analytes that could be determined using

**Table 1**
Results of the linear regression analysis: 24-h concentration vs mean concentration of the corresponding 2-h samples. N indicates the number of data pairs used for the regression.

| Technique | Analyte | Slope | $R^2$ | N |
|---|---|---|---|---|
| β atten. | mass | 1.01 | 0.99 | 21 |
| XRF | Al | 1.02 | 0.98 | 21 |
| XRF | Ca | 1.09 | 0.99 | 21 |
| XRF | Cl | 1.07 | 0.99 | 21 |
| XRF | Fe | 0.98 | 0.98 | 14 |
| XRF | K | 1.07 | 0.99 | 21 |
| XRF | Mg | 1.06 | 0.99 | 21 |
| XRF | Na | 1.09 | 0.97 | 13 |
| XRF | S | 1.05 | 0.98 | 21 |
| XRF | Si | 1.02 | 0.98 | 21 |
| XRF | Ti | 1.04 | 0.98 | 21 |
| IC | $Ca^{++}$ | 0.95 | 0.98 | 21 |
| IC | $Cl^{-}$ | 0.89 | 0.99 | 21 |
| IC | $K^{+}$ | 0.95 | 0.98 | 21 |
| IC | $Mg^{++}$ | 1.04 | 0.96 | 21 |
| IC | $Na^{+}$ | 1.05 | 0.99 | 21 |
| IC | $NH_4^{+}$ | 0.97 | 0.99 | 21 |
| IC | $NO_3^{-}$ | 0.91 | 0.99 | 21 |
| IC | $SO_4^{=}$ | 0.94 | 0.97 | 21 |
| $ICP_{sol}$ | Ba | 0.82 | 0.95 | 15 |
| $ICP_{sol}$ | Cs | 0.92 | 0.96 | 17 |
| $ICP_{sol}$ | Cu | 0.87 | 0.96 | 21 |
| $ICP_{sol}$ | Mg | 0.99 | 0.98 | 15 |
| $ICP_{sol}$ | Mn | 0.84 | 0.94 | 21 |
| $ICP_{sol}$ | Mo | 1.05 | 0.97 | 19 |
| $ICP_{sol}$ | Na | 0.89 | 0.98 | 16 |
| $ICP_{sol}$ | Rb | 0.93 | 0.98 | 18 |
| $ICP_{sol}$ | Sb | 1.08 | 0.97 | 21 |
| $ICP_{sol}$ | Sn | 0.97 | 0.98 | 19 |
| $ICP_{sol}$ | Sr | 0.83 | 0.94 | 16 |
| $ICP_{sol}$ | V | 0.96 | 0.99 | 21 |
| TOA | EC | 1.08 | 0.97 | 21 |
| TOA | OC | 0.86 | 0.98 | 21 |

two different analytical techniques. The results were generally satisfactory, excepting the XRF determination of Na, which was affected by a high amount of data below the detection limit. For these analytes, we selected the analytical technique that provided the higher amount of data above the LOD.

The final dataset included 27 species: total Al, Ca, Fe, K, Mg, Si, Ti (analyzed by XRF), $Cl^{-}$, $NO_3^{-}$, $SO_4^{=}$, $Na^{+}$, $NH_4^{+}$, $K^{+}$, $Mg^{++}$, $Ca^{++}$ (analyzed by IC), the soluble fraction of Ba, Cs, Cu, Mn, Mo, Rb, Sb, Sn, Sr and V (analyzed by $ICP_{sol}$), EC and OC (analyzed by TOA). The descriptive statistics for the 2-h concentration values is reported in Table 2.

On this final dataset, we checked the mass closure for the 2-h samples. 1-h $PM_{10}$ concentrations data obtained during the four SOPs by beta attenuation measurements were averaged on a 2-h basis and compared with the mass concentrations reconstructed by adding the results of the individual chemical analyses. To obtain the reconstructed mass, we considered elements as oxides and multiplied OC by 1.6 to take non-C atoms in the organic molecules into account. The data in Fig. 1 show that a very satisfactory mass closure was obtained: the reconstructed mass accounted for 105 ± 18% of the mass measured by beta attenuation.

## 3. Results

As a first evaluation of the behaviour of the main PM components at the 2-h time scale, we considered the variations in the concentration of the main macro-sources during the four SOPs (Fig. 2). A recurring daily pattern, with higher values during the night and morning, was shown by the three macro-sources of mainly anthropic origin: *secondary inorganics, organics, traffic exhaust*. In particular, high concentrations of *secondary inorganics* were recorded during the first two SOPs, with ammonium

**Table 2**
Descriptive statistics for the 2-h concentration of $PM_{10}$ components during the SOPs.Mass concentration, EC and OC are in μg $m^{-3}$; the other components are in ng $m^{-3}$.

| Technique | Analyte | Mean | Median | 10th | 90th |
|---|---|---|---|---|---|
| β atten. | mass | 30.3 | 25.7 | 13.0 | 54.9 |
| XRF | Al | 170 | 120 | 70 | 310 |
| XRF | Ca | 1490 | 1180 | 430 | 2930 |
| XRF | Fe | 420 | 250 | 50 | 890 |
| XRF | K | 470 | 360 | 200 | 810 |
| XRF | Mg | 250 | 170 | 110 | 520 |
| XRF | Si | 700 | 480 | 180 | 1370 |
| XRF | Ti | 21 | 16 | 11 | 38 |
| IC | $Ca^{++}$ | 1060 | 930 | 410 | 1880 |
| IC | $Cl^{-}$ | 1620 | 500 | 120 | 4700 |
| IC | $K^{+}$ | 340 | 260 | 150 | 600 |
| IC | $Mg^{++}$ | 170 | 96 | 27 | 390 |
| IC | $Na^{+}$ | 1300 | 660 | 230 | 3120 |
| IC | $NH_4^{+}$ | 950 | 760 | 120 | 1960 |
| IC | $NO_3^{-}$ | 3080 | 2350 | 1080 | 5790 |
| IC | $SO_4^{=}$ | 1540 | 1520 | 880 | 2310 |
| $ICP_{sol}$ | Ba | 8 | <LOD | <LOD | 17 |
| $ICP_{sol}$ | Cs | 0.03 | 0.02 | <LOD | 0.07 |
| $ICP_{sol}$ | Cu | 11 | 9 | 4 | 20 |
| $ICP_{sol}$ | Mn | 4 | 4 | 2 | 7 |
| $ICP_{sol}$ | Mo | 0.3 | 0.3 | <LOD | 0.6 |
| $ICP_{sol}$ | Rb | 1.2 | 0.8 | <LOD | 3.0 |
| $ICP_{sol}$ | Sb | 1.6 | 0.55 | 0.23 | 2.6 |
| $ICP_{sol}$ | Sn | 0.18 | 0.14 | 0.04 | 0.32 |
| $ICP_{sol}$ | Sr | 5 | 5 | <LOD | 9 |
| $ICP_{sol}$ | V | 0.7 | 0.6 | 0.2 | 1.5 |
| TOA | EC | 2.5 | 1.6 | 0.57 | 5.4 |
| TOA | OC | 7.0 | 4.9 | 2.2 | 14 |

nitrate often exceeding 30% of the reconstructed $PM_{10}$ mass during the morning hours. Instead, the macro-sources of mainly natural origin (soil, sea) showed a more complex and irregular daily behaviour. In particular, the chemical components released by the sea showed a remarkable concentration increase during the third SOP (March 8–9 and 12–14), accompanied by an increase in the concentration of soil components. On March 13th, sea components constituted up to almost 60% of the reconstructed $PM_{10}$ mass, compared with an average contribution of 2.3% during the first and the second SOPs. As frequently observed in peninsular Italy (Contini et al., 2014) and as confirmed by the analysis of the back-trajectories, the simultaneous increase of sea salt and soil components can be attributed to the transport of African dust loaded with sea-spray components while travelling over the Mediterranean Sea.

These data can be interpreted more clearly by looking at the natural radioactivity values recorded during the four SOPs, shown in Fig. 3 (1-h time pattern). The data referring to the total 2-month study period are reported in Supplementary Material Figure S2.

From a qualitative point of view, natural radioactivity values during the four SOPs were in most cases (except for the two advection periods discussed below) in agreement with the typical daily cycle of the PBL mixing: high values during the night (poor atmospheric mixing) and low values during daytime hours (convective turbulence). The first two SOPs were characterized by atmospheric stability conditions, typical of the winter season. These conditions were reflected in high natural radioactivity values during the night but also during the daytime (see the case of February 17th) (Kikaj et al., 2020). A reduced mixing of the lower atmosphere during the central hours of the day is generally responsible for very high concentration of pollutants, especially those of secondary formation. As shown in Fig. 2, during the first two SOPs high concentration values were, in fact, recorded for traffic components, organics and, in particular, secondary inorganics.

The atmospheric conditions during the last two SOPs were more variable, with an alternation of moderate stability on March 10, 14 and 24–28, and advection on March 12–13 (from the early afternoon of March 11th) and 22–23. During advection episodes, the daily cycle of natural radioactivity is impacted not only by changes in the mixing

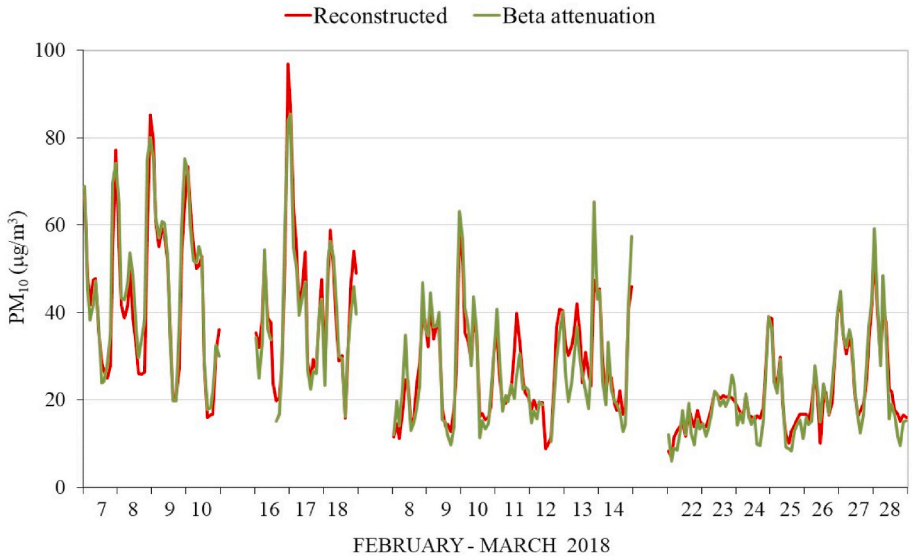


**Fig. 1.** Comparison of $PM_{10}$ mass concentration measured by the beta attenuation method and reconstructed by adding individual chemical analyses of PM components.

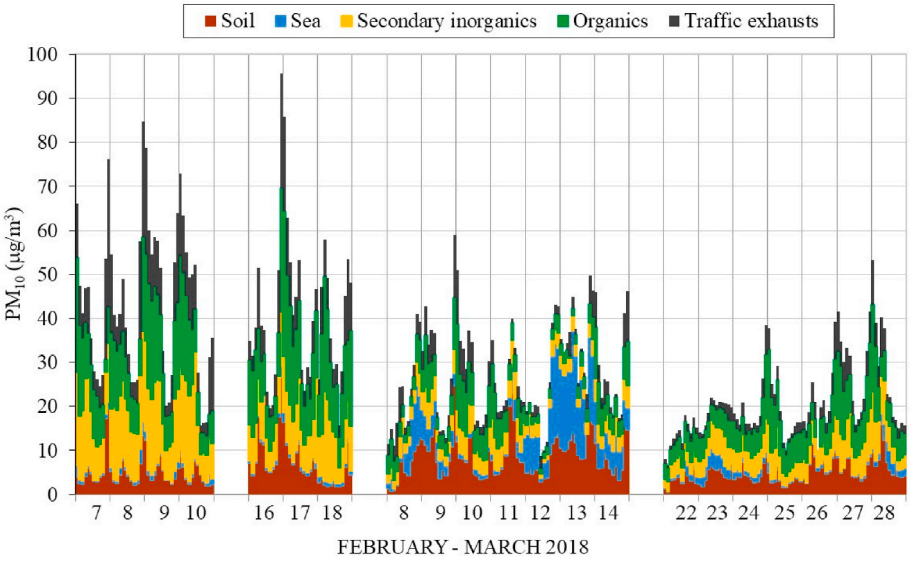


**Fig. 2.** Time pattern of the macro-sources of $PM_{10}$ at the time scale of 2-h.

depth but also by the geological characteristics of the area the air masses have passed over. This is particularly true if the wind is blowing from coastal regions, where the Radon exhalation rate is low. The two advection events considered in this study differed in the wind direction: during the first episode, the wind blew from the coast (S– SW; very low radioactivity values), causing a remarkable increase of the *sea* component of $PM_{10}$, while during the second one it blew from N-NE, bringing continental air masses to the receptor site. The time series of the main meteorological parameters during the SOPs are reported in Supplementary Material Figure S3. The back-trajectories of the air masses during the two episodes are reported in Supplementary Material Figure S4.

It is worth noting that the number of daylight hours was gradually increasing during the four SOPs, with an average value of 10 h 27 m and 12 h 00 m during the first and last two SOPs, respectively. This increase resulted in different time variations in the thickness of the lower boundary layer and thus in the time pattern of natural radioactivity and pollutants concentration.

Following the above analysis, we grouped the 21 days of observation into three clusters: Advection period (March 12–13 and 22–23), February stability period and March stability period. Natural radioactivity data were averaged on a 2-h basis to fit PM composition data. The daily variation of natural radioactivity during the three clusters is shown in Fig. 4 (mean and standard deviation). The three patterns were very different: low values and almost flat trend for the advection period, night-time increase and low values during the central hours of the day for the two stability periods, with a clear difference between February and March (broader time window in March, due to the increased number of daylight hours). It is worth underlying that these three clusters are not quantitatively related to the height of the mixed layer. Still, they give a qualitative indication of the mixing properties of the lower boundary layer that may influence the build-up of pollutant concentration.

Fig. 5 shows the main meteorological parameters during the study period grouped according to the same three clusters. As expected, the velocity of the wind was higher during the advection days and very low during the nights of the stability periods. From the late morning to

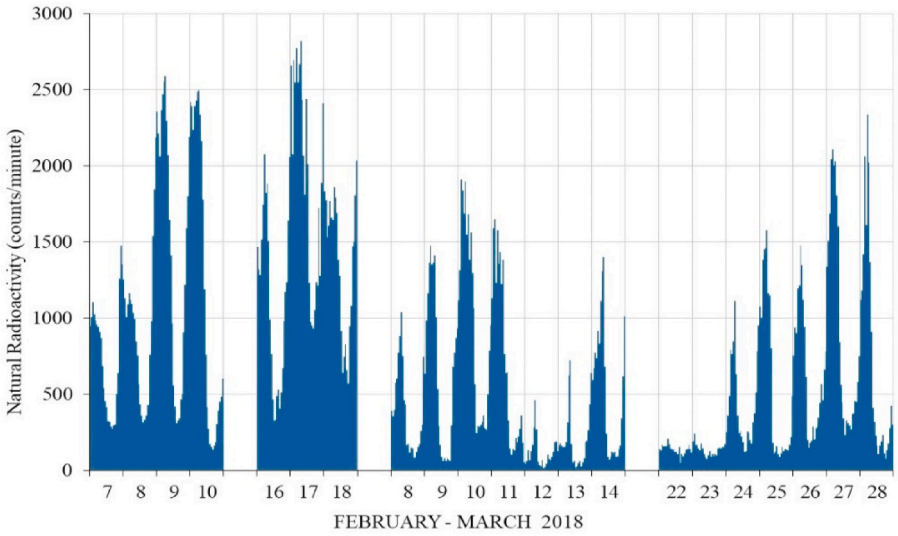


**Fig. 3.** 1-h time pattern of natural radioactivity during the four SOPs.

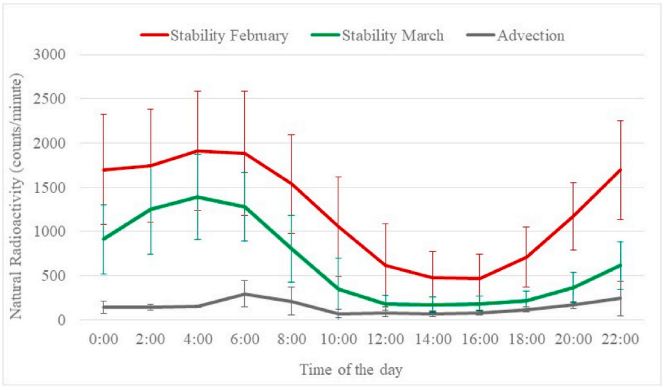


**Fig. 4.** 2-h variation of natural radioactivity during the four SOPs:mean value and standard deviation for the three clusters.

sunset the velocity of the wind increased as a consequence of the sea-breeze blowing from the S-SW sector. In the lower right panel, the two dotted lines indicate the wind direction during the advection period of March 12–13 (S-SE, Advection 1) and 22–23 (N-NE, Advection 2).

To compare the typical daily pattern of natural radioactivity with those of PM components that were representative of PM sources, we run an exploratory Principal Component Analysis (PCA), using the statistical software CAT (Chemometric Agile Tool, based on the R-project for statistical computing, Leardi et al.,). Five components were extracted, able to explain 75.5% of the total variance in the dataset. The loadings are reported in Supplementary Material Table S3.

Fig. 6 shows the Score plot and Loading plot of components 1 and 2. Component 1 explained 34.2% of the variance, had the highest impact on PM concentration and was characterized by PM compounds of anthropic origin. Component 2 explained 18.5% of the variance and was mainly related to the variation in the concentration of secondary species. Several groups of compounds could be detected in the loading plot, well separated from each other: soluble chloride, sodium and magnesium (blue circle), originated by the sea aerosol; - Al, Si, Ti, Ca, the insoluble fraction of Mg and K and the soluble fraction of Sr (brown circle), which are all soil components; - Fe and the soluble fraction of Mo, V, Sb, Sn, Cu, Mn, Ba (black circle), released by exhaust and non-exhaust traffic emission; - the soluble fraction of Cs, Rb and K (green circle), excellent tracers of biomass burning; - sulphate, ammonium and nitrate (yellow circle), which are secondary species. OC, which includes a huge number of chemical species, was very close to the secondary inorganic species group, indicating that the secondary pathway was responsible for the formation of most of these compounds. Interestingly, EC and mass concentration were close to the group of biomass burning, highlighting that domestic heating is a relevant source of PM and that elemental carbon is substantially released by this source. Natural radioactivity was very close to inorganic and organic secondary species. This is a first indication that these PM components were the most sensitive to the variations in the height of the boundary layer.

The samples collected during the three clusters of periods (Advection, Stability February and Stability March) were distributed in different areas of the score plot: the samples taken during the advection periods were distributed in the area corresponding to the sea aerosol in the loading plot, while those taken during Stability February gathered in the area corresponding to secondary species. Also, when considering samples taken during night (n) and day (d) hours, it was evident that the samples collected during the night of both February and March stability periods showed higher values in component 1.

To understand the role of atmospheric mixing in determining the daily time pattern of PM components, we grouped the 2-h data collected during the SOPs for each of the 27 examined components according to the three clusters of periods and compared the three obtained daily patterns with those of natural radioactivity. In Fig. 7, we report the results obtained for some interesting components, selected as representative members of each group identified by the PCA. The rationale for this analysis is that the concentration of any component having a constant emission rate and no chemical transformations should be mainly governed by the mixing properties of the PBL and show the same time pattern of natural radioactivity. Any difference indicates variations in the emission rate throughout the day or significant chemical or physical transformations.

The daily time patterns of EC, Fe and Si concentration are reported in panels A, B and C of Fig. 7, respectively. The concentration of EC showed a minimum between 12:00 and 18:00, during the period of maximum mixing of the atmosphere recorded by natural radioactivity (Fig. 4). During the evening and the early night, EC concentration rapidly increased, due to the stabilization of the lower atmosphere but also to the increase in the emission of this component by both traffic exhaust (rush hour) and biomass burning (Perrino et al., 2002, 2010, 2019; Catrambone et al., 2003). The relative increase in the rate of evening/early night accumulation of EC compared to radioactivity is a good indication of the increasing strength of these two EC source during these time periods. After midnight, despite the further increase in atmospheric

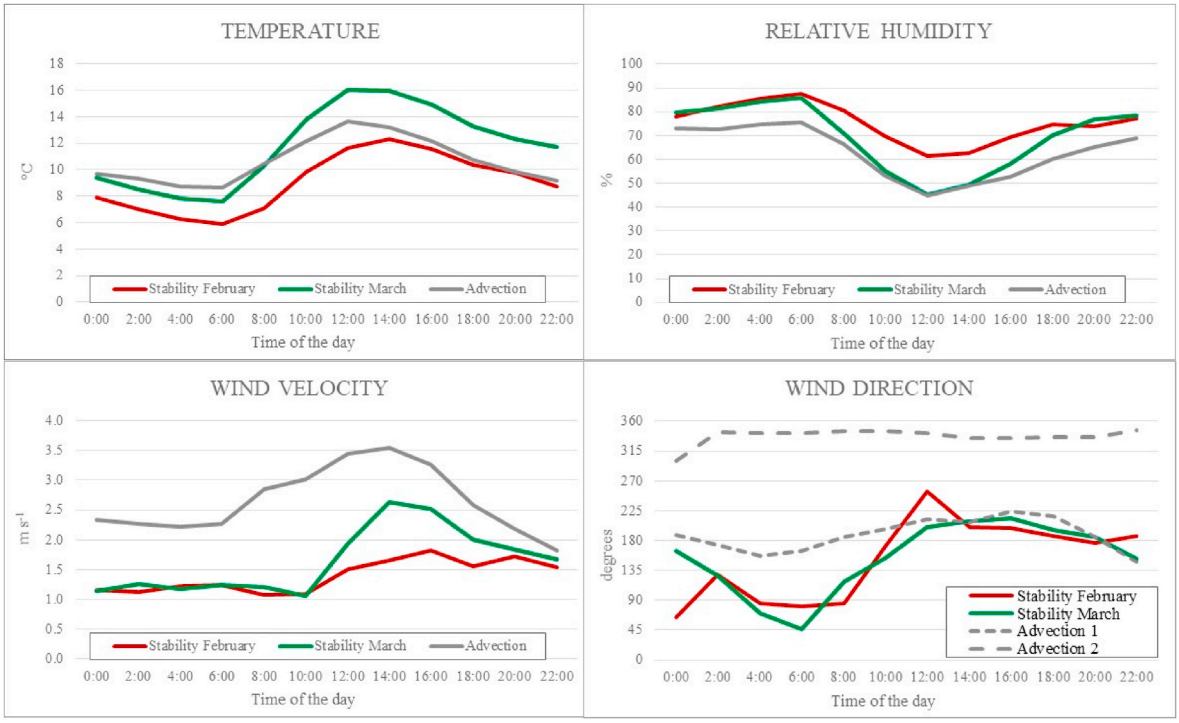


**Fig. 5.** 2-h variation in the main meteorological parameters during the four SOPs:mean value for the three clusters.

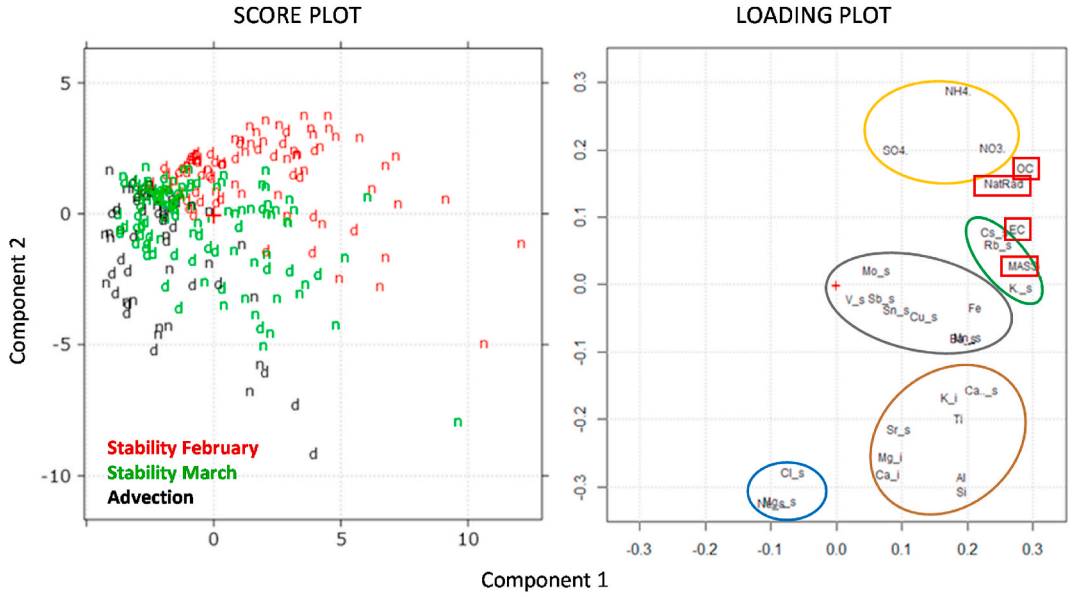


**Fig. 6.** Principal Component Analysis: score plot and loading plot of components 1 and 2. In the score plot, *n* and *d* indicate night-time and daytime hours, respectively. _i indicates the insoluble fraction, calculated as the difference between XRF and IC determinations; _s indicates the soluble fraction, determined by IC (K, Mg, Ca, Cl) or ICP-MS.

stability, EC concentration decreased due to the substantial reduction in its emission rate. An increase was observed again between 6:00 and 10:00; in this case, the strengthening of the emission rate (morning rush hour and switch-on of the heating appliances) was counterbalanced by the dilution of the atmosphere (natural radioactivity pattern shows a decreasing trend) and resulted in a lower concentration with respect to the evening. As in the case of natural radioactivity, EC concentration recorded during the Stability February cluster was higher than during Stability March, which was higher than during Advection, indicating a crucial role of the atmospheric mixing in determining the concentration of this PM component.

Fe concentration (panel B) showed a very similar daily pattern. The most significant difference with respect to EC was the lower minimum concentration during the last hours of the night (2:00–6:00). This difference might be attributed to the more rapid deposition of particles containing Fe, produced by brake pads erosion, which are heavier than carbon particles. Also, the lower wind speed during the night may be responsible of a lower resuspension of these particles. A third possible explanation could be the less frequent use of brakes during the night, compared to rush hours.

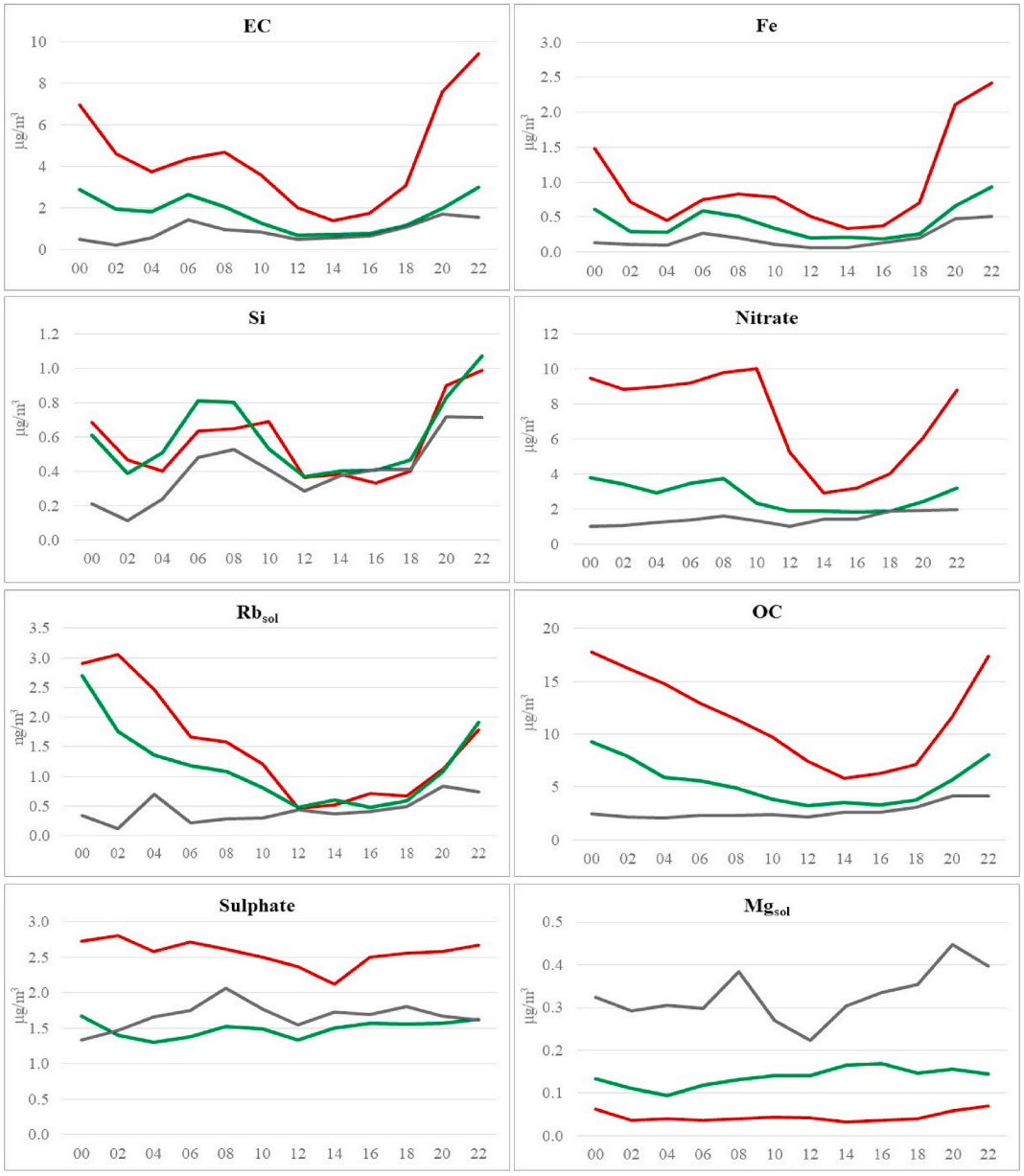


**Fig. 7.** 2-h variation in the concentration of selected PM components during the four SOPs: mean value for the three clusters (Advection: black line; February Stability: green line; March Stability: red line). (For interpretation of the references to colour in this figure legend, the reader is referred to the Web version of this article.)

The concentration of Si (panel C) showed a pattern similar to those of EC and Fe. In urban areas, the release of soil components in the atmosphere is due to the production by wind erosion but also to the resuspension of deposited particles, due to both the action of wind and the transit of vehicles. We, therefore, recorded a concentration increase after sunset, due to both atmospheric stabilization and rush hour, a decrease after midnight similar to the case of EC (light particles), and a new increase after sunrise, due to the increase in traffic.

The decrease observed for EC, Fe and Si (and other soil components) between 2:00 and 6:00, when natural radioactivity reaches its maximum (Fig. 4), indicates a strong reduction in the emission strength of these species. However, it might also be partially due to a very gentle katabatic drainage flow from N-NE to SW, away from the mountains (Fig. 5). This advection effect is of modest magnitude, as it is slightly visible in the time pattern of the other components in Fig. 6 (e.g. nitrate, sulphate).

In the case of Si and all soil components, unlike EC and Fe, the pattern recorded during the Advection cluster was closer to those recorded during stability periods, and there were no substantial differences between February and March Stability clusters. This finding underlines the role of the wind in determining the concentration variations for these PM components.

A very different pattern was recorded for nitrate concentration (panel D). In this case, high concentrations were kept during the whole night and morning (until the period 10:00–12:00), and there was a considerable difference between the values recorded during the Stability February and the Stability March clusters. This finding confirms that the mixing properties of the atmosphere play a key role in determining the atmospheric concentration of secondary components such as ammonium nitrate and that this particular component is much more sensitive than others to atmospheric stability (Quan et al., 2014; Liu et al., 2018). Other authors already recorded a persistence of high nitrate concentration during the late morning hours and attributed it to the lower temperature and higher humidity, which favours $NH_4NO_3$ over gaseous

precursors ($NH_3$ and $HNO_3$), but also to the increased availability of ammonia, emitted by vehicle exhausts, during morning hours (Perrino et al., 2002, 2015; Takahama et al., 2004; Revuelta et al., 2012). It is worth underlining that in the geographical area of Rome, which is, in general, characterized by a good mixing of the lower PBL due to the proximity to the sea, the conditions leading to massive production of secondary pollutants are not frequent, of short duration (a few days) and limited to the winter months (Perrino et al., 2020).

The soluble fraction of Rb, a reliable tracer of biomass burning emission (Vicente and Alves, 2018; Perrino et al., 2019), showed an increase during the evening and a slow decrease during the night and morning (panel E). This pattern is consistent with the behaviour of a source that is switched on during the evening and the first hours of the night, and again during the early morning, as it is plausible for domestic heating. The difference in the diurnal pattern between $Rb_{sol}$ and EC is because the first species is contributed by biomass burning only, while in the case of EC the contribution of biomass burning superimposes to that of traffic. In the loading plot of the PCA analysis, in fact, EC data are very close to the biomass burning tracers ($Rb_{sol}$, $Cs_{sol}$ and $K_{sol}$, Fig. 6), showing that the contribution of this source to total EC concentration may be very relevant.

The pattern of bulk OC (panel F) reflected the pattern combination of the many components that constitute the organic aerosol, mainly secondary species and primary species from biomass burning and traffic emission. The difference between the Stability February and the Stability March clusters indicates a main contribution of the secondary organic aerosol, and the high values recorded during the night and morning hours point at a relevant contribution of biomass burning. The absence of an apparent morning increase between 6:00 and 10:00 indicates that the above sources dominate over traffic emissions.

In the case of sulphate (panel G), similarly to what observed for nitrate, there was a difference between the pattern recorded during the Stability February and the Stability March clusters, as it is expected for a secondary component such as ammonium sulphate. However, over the 24 h there were no substantial concentration variations. This flat pattern may be due to the fact that ammonium sulphate, of photochemical origin, is mainly produced during daylight hours, when the mixing depth is greater and the pollutants are more diluted. Also, it should be considered that in the area of Rome there are no important industrial activities and no power plants, and most of the emission of sulphate precursors is not local.

The last panel in Fig. 7 (panel H) shows the behaviour of a PM component whose time pattern is not influenced by the atmospheric mixing and is thus not related to natural radioactivity. In the case of soluble Mg, a tracer of the sea aerosol, there was no typical daily pattern, and the concentration variations depended on when each transport event from the coast occurred. Given the role of wind intensity in determining sea-salt events, this was the only case when the concentration during the Advection cluster was much higher than during the Stability clusters.

## 4. Conclusions

Natural radioactivity confirmed to be a reliable tool for studying the influence of the mixing depth on the build-up of PM components. The comparison between its time pattern and those of the concentration of PM components at 2-h time resolution gave insight into the behaviour of some PM sources and allowed uncoupling of the effect of emission and atmospheric dilution in determining pollutants concentration data.

The approach adopted in this study led to a more comprehensive characterization of PM sources in terms of chemical composition and daily profiles and allowed to highlight the primary role of the mixing depth in determining the concentration of PM constituents.

Ammonium salts and organics were the most sensitive PM components to periods of increased atmospheric stability; soil and biomass burning components were more sensitive to the daily development of the mixed layer. For traffic tracers, a difference in the night-time concentration was shown for Fe and EC, due to the different dimensions and density of the particles, influencing gravitational settling.

Further studies are needed to further reduce the observation time of PM components, using high-resolution continuous monitoring instrumentation, and to focus on the many sources contributing to the burden of organic components.

## Author statement

C. Perrino: Conceptualization; Methodology; Validation; Formal analysis; Writing – original draft; Writing – review & editing; Visualization; Supervision; M. Giusto: Investigation; Formal analysis; Data curation; T. Sargolini: Investigation; Resources; G. Calzolai: Investigation; Resources; S. Canepari: Conceptualization; Methodology; Writing – review & editing.

## Declaration of competing interest

The authors declare that they have no known competing financial interests or personal relationships that could have appeared to influence the work reported in this paper.

## Acknowledgements

The authors are grateful to F. Lucarelli and its research group (INFN, Florence) and to P. Avino and M. Manigrasso (INAIL, Rome) for providing some of the instrumentation used in this work. The authors also thank M. Catrambone (CNR-ISPC, Milano), S. Pareti and E. Rantica (CNR-IIA) and L. Massimi (Sapienza University) for analytical support.

## Appendix A. Supplementary data

Supplementary data to this article can be found online at https://doi.org/10.1016/j.chemosphere.2022.134272.

## References

Allegrini, I., Febo, A., Pasini, A., Schiarini, S., 1994. Monitoring of the nocturnal mixed layer by means of particulate radon progeny measurement. J. Geophys. Res. 99, 18765–18777.

Belis, C.A., Pikridas, M., Lucarelli, F., Petralia, E., Cavalli, F., Calzolai, G., Berico, M., Sciare, J., 2019. Source apportionment of fine PM by combining high time resolution organic and inorganic chemical composition datasets. Atmos. Environ. X 3, 100046.

Bigi, A., Bianchi, F., De Gennaro, G., Di Gilio, A., Fermo, P., Ghermandi, G., Prévôt, A.S. H., Urbani, M., Valli, G., Vecchi, R., Piazzalunga, A., 2017. Hourly composition of gas and particle phase pollutants at a central urban background site in Milan, Italy. Atmos. Res. 186, 83–94.

Comune di Roma, 2017. Piano Urbano Della Mobilità Sostenibile. https://www.comune.roma.it/web-resources/cms/documents/PUMS_roma_vol1.pdf.

Canepari, S., Cardarelli, E., Pietrodangelo, A., Strincone, M., 2006. Determination of metals, metalloids and non-volatile ions in airborne particulate matter by a new two-step sequential leaching procedure: Part B: Validation on equivalent real samples. Talanta 69 (3), 588–595.

Canepari, S., Perrino, C., Astolfi, M.L., Catrambone, M., Perret, D., 2009. Determination of soluble ions and elements in ambient air suspended particulate matter: inter-technique comparison of XRF, IC and ICP. for sample-by-sample quality control. Talanta 77, 1821–1829.

Catrambone, M., Perrino, C., Di Menno Di Bucchianico, A., 2003. Gaseous ammonia from traffic emissions in the urban area of Rome. WIT Trans. Ecol. Environ. 66.

Castro, L.M., Pio, C.A., Harrison, R.M., Smith, D.J.T., 1999. Carbonaceous aerosol in urban and rural European atmospheres: estimation of secondary organic carbon concentrations. Atmos. Environ. 33, 2771–2781.

Chow, J.C., Lowenthal, D.H., Chen, L.W.A., Wang, X., Watson, J.G., 2015. Mass reconstruction methods for PM 2.5: a review. Air Qual. Atmos. Hlth. 8 (3), 243–263.

Chambers, S.D., Williams, A.G., Crawford, J., Griffiths, A.D., 2015. On the use of Radon for quantifying the effects of atmospheric stability on urban emissions. Atmos. Chem. Phys. 15, 1175–1190.

Contini, D., Cesari, D., Genga, A., Siciliano, M., Ielpo, P., Guascito, M.R., Conte, M., 2014. Source apportionment of size-segregated atmospheric particles based on the major water-soluble components in Lecce (Italy). Sci. Total Environ. 472, 248–261.

D'Alessandro, A., Lucarelli, F., Mandò, P.A., Marcazzan, G., Nava, S., Prati, P., Valli, G., Vecchi, R., Zucchiatti, A., 2003. Hourly elemental composition and sources

identification of fine and coarse PM10 particulate matter in four Italian towns. J. Aerosol Sci. 34, 243–259.
Desideri, D., Roselli, C., Feduzi, L., Meli, M.A., 2006. Monitoring the atmospheric stability by using radon concentration measurements: a study in a Central Italy site. J. Radioanal. Nucl. Chem. 270, 523–530.
Duenas, C., Perez, M., Fernandez, M.C., Carretero, J., 1996. Radon concentrations in surface air and vertical atmospheric stability of the lower atmosphere. J. Environ. Radioact. 31, 87–102.
Emeis, S., Schafer, K., Munkel, C., 2008. Surface-based remote sensing of the mixing-layer height – a review. Meteorol. Z. 17, 621–630.
Farao, C., Canepari, S., Perrino, C., Harrison, R.M., 2014. Sources of PM in an Industrial Area: comparison between receptor model results and semiempirical calculations of source contributions. Aerosol Air Qual. Res. 14, 1558–1572.
Gao, J., Peng, X., Chen, G., Xu, J., Shi, G.L., Zhang, Y.C., Feng, Y.C., 2016. Insights into the chemical characterization and sources of PM2. 5 in Beijing at a 1-h time resolution. Sci. Total Environ. 542, 162–171.
Gregorič, A., Drinovec, L., Ježek, I., Vaupotič, J., Lenarčič, M., Grauf, D., Wang, L., Mole, M., Stanič, S., Močnik, G., 2020. The determination of highly time-resolved and source-separated black carbon emission rates using radon as a tracer of atmospheric dynamics. Atmos. Chem. Phys. 20 (22), 14139–14162.
Griffith, A.D., Parkes, S.D., Chambers, S.D., McCabe, M.F., Williams, A.G., 2013. Improved mixing height monitoring through a combination of lidar and radon measurements. Atmos. Meas. Tech. 6, 207–218.
Guedalia, D., Ntsila, A., Druihlet, A., Fontan, J., 1980. Monitoring of the atmospheric stability above an urban and suburban site using Sodar and radon measurements. J. Appl. Meteorol. 19, 839–848.
Kidwell, C.B., Ondov, J.M., 2004. Elemental analysis of sub-hourly ambient aerosol collections. Aero. Sci. Technol. 38, 205–218.
Kikaj, D., Chambers, S.D., Kobal, M., Crawford, J., Vaupotič, J., 2020. Characterizing atmospheric controls on winter urban pollution in a topographic basin setting using Radon-22. Atmos. Res. 237, 104838.
Leardi, R., Melzi, C., Polotti, G.. CAT (chemometric agile tool). Available online: http://gruppochemiometria.it/index.php/software. (Accessed 17 June 2021).
Li, Y., Liu, B., Xue, Z., Zhang, Y., Sun, X., Song, C., Dai, Q., Fu, R., Tai, Y., Gao, J., Zheng, Y., Zheng, Y., 2020. Chemical characteristics and source apportionment of PM2.5 using P.M.F. modelling coupled with 1-hr resolution online air pollutant dataset for Linfen, China. Environ. Pol. 114532.
Liu, Q., Jia, X., Quan, J., Li, J., Li, X., Wu, Y., Wang, Z., Liu, Y., 2018. New positive feedback mechanism between boundary layer meteorology and secondary aerosol formation during severe haze events. Sci. Rep. 8 (1), 1–8.
Nath, S., Patil, R.S., 2006. Prediction of air pollution concentration using an in situ real time mixing height model. Atmos. Environ. 40, 3816–3822.
Nicolás, J., Lucarelli, F., Galindo, N., Yubero, E., Crespo, J., Calzolai, G., Nava, S., 2020. Impact of traffic flows and meteorological events on the hourly elemental composition of fine and coarse particles at an urban site. Aerosol Air Qual. Res. 20 (5), 991–1001.
Pancras, J.P., Landis, M.S., Norris, G.A., Vedantham, R., Dvonch, J.T., 2013. Source apportionment of ambient fine particulate matter in Dearborn, Michigan, using hourly resolved PM chemical composition data. Sci. Total Environ. 448, 2–13.
Pasini, A., Perrino, C., Zujíc, A., 2003. Non-linear atmospheric stability indices by neural network modelling. Nuovo Cimento C 26, 633–638.
Perrino, C., Pietrodangelo, A., Febo, A., 2001. An atmospheric stability index based on radon progeny measurements for the evaluation of primary urban pollution. Atmos. Environ. 35, 5235–5244.
Perrino, C., Catrambone, M., Di Menno Di Bucchianico, A., Allegrini, I., 2002. Gaseous ammonia in the urban area of Rome and its relationship with traffic emissions. Atmos. Environ. 36, 5385–5394.
Perrino, C., Catrambone, M., Pietrodangelo, A., 2008. Influence of atmospheric stability on the mass concentration and chemical composition of atmospheric particles: a case study in Rome. Italy. Environ. Int. 34, 621–628.
Perrino, C., Canepari, S., Pappalardo, S., Marconi, E., 2010. Time-resolved measurements of water-soluble ions and elements in atmospheric particulate matter for the characterization of local and long-range transport events. Chemosphere 80, 1291–1300.
Perrino, C., Catrambone, M., Dalla Torre, S., Rantica, E., Sargolini, T., Canepari, S., 2014. Seasonal variations in the chemical composition of particulate matter: a case study in the Po Valley. Part I: macro-components and mass closure. Environ. Sci. Pollut. Res. 21, 3999–4009.
Perrino, C., Catrambone, M., Farao, C., Salzano, R., Esposito, G., Giusto, M., Montagnoli, M., Marini, A., Brinoni, M., Canepari, S., 2015. Improved time-resolved measurements of inorganic ions in Particulate Matter by PILS-IC integrated with a sample pre-concentration system. Aerosol Sci. Technol. 49, 521–530.
Perrino, C., Catrambone, M., Farao, C., Canepari, S., 2016. Assessing the contribution of water to the mass closure of PM10. Atmos. Environ. 140, 555–564 (c).
Perrino, C., Tofful, L., Dalla Torre, S., Sargolini, T., Canepari, S., 2019. Biomass burning contribution to $PM_{10}$ concentration in Rome (Italy): seasonal, daily and two-hourly variations. Chemosphere 222, 839–848.
Perrino, C., Catrambone, M., Canepari, S., 2020. Chemical composition of PM10 in 16 urban, industrial and background sites in Italy. Atmosphere 11 (5), 479.
Porstendorfer, J., 1994. Properties and behaviour of Radon and thoron and their decay products in the air. J. Aerosol Sci. 25, 219–263.
Quan, J., Tie, X., Zhang, Q., Liu, Q., Li, X., Gao, Y., Zhao, D., 2014. Characteristics of heavy aerosol pollution during the 2012–2013 winter in Beijing, China. Atmos. Environ 88, 83–89.
Revuelta, M.A., Harrison, R.M., Núñez, L., Gomez-Moreno, F.J., Pujadas, M., Artíñano, B., 2012. Comparison of temporal features of sulphate and nitrate at urban and rural sites in Spain and the UK. Atmos. Environ. 60, 383–391.
Salzano, R., Pasini, A., Casasanta, G., Cacciani, M., Perrino, C., 2016. Quantitative interpretation of air radon progeny fluctuations in terms of stability conditions in the atmospheric boundary layer. Boundary-Layer Meteorol. 160, 529–550.
Sesana, L., Caprioli, E., Marcazzan, G.M., 2003. Long period study of outdoor radon concentration in Milan and correlation between its temporal variation and dispersion properties of the atmosphere. J. Environ. Radioact. 65, 147–160.
Seibert, P., Beyrich, F., Gryning, S.-E., Joffre, S., Rasmussen, A., Tercier, P., 2000. Review and intercomparison of operational methods for the determination of the mixing height. Atmos. Environ. 34, 1001–1027.
Stull, R.B., 1988. An Introduction to Boundary Layer Meteorology. Kluwer Academic Publishers.
Takahama, S., Wittig, A.E., Vayenas, D.V., Davidson, C.I., Pandis, S.N., 2004. Modeling the diurnal variation of nitrate during the pittsburgh air quality study. J. Geophys. Res. Atmos. 109 (D16).
Certificate, T.Ü.V., 12 April 2018. 0000028733_02; TÜV Rheinland Energy GmbH. Köln, Germany.
Vecchi, R., Bernardoni, V., Fermo, P., Lucarelli, F., Mazzei, F., Nava, S., Prati, P., Piazzalunga, A., Valli, G., 2009. 4-hours resolution data to study PM10 in a "hot spot" area in Europe. Environ. Monit. Assess. 154 (1), 283–300.
Vecchi, R., Piziali, F.A., Valli, G., Favaron, M., Bernardoni, V., 2019. Radon-based estimates of equivalent mixing layer heights: a long-term assessment. Atmos. Environ. 197, 150–158.
Vicente, E.D., Alves, C.A., 2018. An overview of particulate emissions from residential biomass combustion. Atmos. Res. 199, 159–185.
Vogelezang, D.H.P., Holtslag, A.A.M., 1996. Evolution and model impacts of alternative boundary layer formulations. Boundary-Layer Meteorol. 81, 245–269.
Wang, F., Chambers, S.D., Zhang, Z., Williams, A.G., Deng, X., Zhang, H., Lonati, G., Crawford, J., Griffiths, A.D., Ianniello, A., Allegrini, I., 2016. Quantifying stability influences on air pollution in Lanzhou, China, using a radon-based "stability monitor": seasonality and extreme events. Atmos. Environ. 145, 376–391.
Williams, A.G., Chambers, S.D., Conen, F., Reimann, S., Hill, M., Griffiths, A.D., Crawford, J., 2016. Radon as a tracer of atmospheric influences on traffic-related air pollution in a small inland city. Tellus B 68 (1), 30967.